International Journal of GEOMATE, Aug. 2019, Vol.17, Issue 60, pp.62- 69
Geotec., Const. Mat. & Env., DOI: https://doi.org/10.21660/2019.60.4733
ISSN: 2186-2982 (Print), 2186-2990 (Online), Japan

DEVELOPMENT OF DROUGHT RISK ANALYSIS PLATFORM USING MULTIPLE SATELLITE SENSORS

*Mongkol Raksapatcharawong and Watcharee Veerakachen

Chulabhorn Satellite Receiving Station, Faculty of Engineering, Kasetsart University, Thailand

*Corresponding Author, Received: 28 Dec. 2018, Revised: 02 Feb. 2019, Accepted: 21 Feb. 2019

ABSTRACT: Drought, due to climate change, has in recent years become more severe. Capability to monitor drought conditions and to assess drought risk is essential to the development of an effective drought adaptation plan, especially for an agricultural country like Thailand. Current drought monitoring is provided by separate indices such as Standardized Precipitation Index (SPI), Soil Moisture Index (SMI) and Moisture Available Index (MAI), calculated from weather station datasets which are not easily comprehensible to users. This research develops a countrywide integrated satellite-based drought model consisting of three parameters: accumulated estimated rainfall generated from FY-2E satellite data, the difference in Land Surface Temperature (LST) and Normalized Difference Vegetation Index (NDVI) generated from MODIS. A simple drought hazard is introduced as a multiple linear regression model (R^2=0.795) of these satellite products, calibrated with daily soil moisture measurements in 2015. Consequently, drought conditions are represented by the Drought Hazard Index (DHI) whose assigned integer values are from –3 (extremely dry) to +3 (extremely wet), according to the defined thresholds (presently at 0.05, 0.15, 0.30, 0.70, 0.80, and 0.95) of the cumulative distribution function (CDF) of drought hazard values. The model is validated with 426 countrywide drought situations announced by the Department of Disaster Prevention and Mitigation (DDPM), during the drought season of 2016, yielding a 0.96 probability of detection. Subsequently, the model outputs are processed with relevant GIS data, which are agricultural and irrigation areas to represent drought exposure and vulnerability respectively, to generate a drought risk map for further analysis and planning. This platform can benefit not only policymakers but also the farmers themselves.

Keywords: Drought model, FY-2E, GIS, MODIS, Multiple linear regression

1. INTRODUCTION

Drought is a major recurring natural disaster that poses a threat to water and food security [1], environmental problems as well as economic risks, especially for the agricultural sector. Based on their impact, droughts are classified into four types and usually occur in a particular order, which is meteorological drought, agricultural drought, hydrological drought and socioeconomic drought. Meteorological drought is caused by a deficit in precipitation, which subsequently impacts on soil water content, leading to the agricultural drought that results in plant water stress and reduced biomass and yield. Due to low recharge from the soil to water features, hydrological drought occurs when stream flow, reservoir storage and groundwater levels are in shortage. Eventually, the socioeconomic drought will take place if the phenomena are prolonged until water demand increases and water stress is intensified by human activities [2-4].

Drought monitoring and early warning are crucial components for mitigation and adaptation plans [4]. Drought management typically responds to crisis after impacts have occurred. Moreover, drought relief provided to those affected decreases socioeconomic capabilities of adaptation to drought disasters [5]. Thus, practical drought monitoring and risk assessment are essential to developing an effective drought early warning and adaptation plan in which potential victims are able to get involved, leading to proactive and effective drought management which can actually reduce damaging impacts.

Traditional drought monitoring utilizes several indices such as the Standardized Precipitation Index (SPI), Soil Moisture Index (SMI), and Moisture Available Index (MAI). Each represents various aspects of drought and has been widely used. The SPI presents a rainfall anomaly as a normalized variable by probabilistically comparing accumulated rainfall over a time period with a historical rainfall period. The SMI indicates soil water content, while the MAI determines the influence of water adequacy on yields. However, the indices derived from weather stations are point-based and insufficient to monitor drought on a regional scale [6]. Consequently, remote sensing satellite data has become a valuable tool and assumed a significant role in drought monitoring due to its grid-based feature providing spatial information on drought even at a global scale. Satellite-based data has an additional advantage

compared to ground-based observation in that various types of data records and products can be utilized in developing advanced drought monitoring with multiple data sources.

Various satellite-based drought indices have been developed to monitor drought and can be categorized into three main perspectives. The first one provides precipitation information, of which SPI is the most widely used. Its computation requires data from infrared (IR) sensors of a geostationary (GEO) satellite (for higher temporal resolution) and from passive microwave (PWM) sensors of a low earth orbit (LEO) satellite, (for more accurate rainfall estimate). Currently, there are several satellite-based precipitation products available including Precipitation Estimation from Remotely Sensed Information using Artificial Neural Networks (PERSIANN) [7], Tropical Rainfall Measuring Mission (TRMM) [8], CPC Morphing Technique (CMORPH) [9] and Global Satellite Mapping of Precipitation (GSMaP) [10]. However, these products have a relatively short length of records, which impose a limitation on SPI calculation.

The second category of satellite-based indices is based on Land Surface Temperature (LST) which is related to soil water content, such as the Temperature Condition Index (TCI) and Normalized Difference Temperature Index (NDTI) [11,12]. The last category assesses drought based on observed changes in vegetation conditions with indices typically derived from the Normalized Difference Vegetation Index (NDVI), such as the Transformed Vegetation Index (TVI), the Standardized Vegetation Index (SVI), and the Vegetation Condition Index (VCI) [13-15]. The combination of LST and NDVI has been investigated in several works to provide more robust characteristics of a drought phenomenon [16]. LST-NDVI based indices have been applied over different landscapes with varying degrees of success, e.g., Temperature Vegetation Dryness Index (TVDI) and Vegetation Temperature Condition Index, (VTCI) [17,18].

Drought risk is composed of a disaster forming environment and disaster bearing body [19,20]. Drought damage can be lessened or magnified by the degree of drought vulnerability [21]. Drought exposure is defined as its livelihoods and assets in an area in which drought hazard events may occur while drought vulnerability is defined as the propensity of exposed elements to suffer adverse effects when impacted by a drought event. As a result, drought risk is assessed based on the product of hazard, exposure and vulnerability, indicating the probability of harmful consequences [22].

This work introduces a simple satellite-based drought hazard model that combines all drought-related aspects including rainfall, soil moisture and vegetation condition. The model inputs are derived from satellite products. Drought hazard values obtained from the model were collected to generate a probabilistic function. The function was defined to indicate levels of Drought Hazard Index (DHI) that can be shown on a map for easy interpretation. By combining DHI with relevant GIS data, which are agricultural areas from Land Development Department (LDD) to represent drought exposure factor and irrigation areas from Royal Irrigation Department (RID) to represent a factor inversely proportional to drought vulnerability, our platform can automatically generate and publish a drought risk map at http://csrs.ku.ac.th/wegis/product/kurdi. In addition, interest users can download the map in GeoTIFF format for their customized processing. The satellite-based products and drought risk map are updated every 10 days.

2. METHODOLOGY

The satellite-based drought hazard model consists of three dekadal (10 days) satellite data products which are accumulated rain estimate, difference LST, and NDVI values. The relationship between these input parameters and the drought hazard values was investigated using a multiple linear regression technique. Ground-based and reference datasets were collected to be used for model calibration and comparison analysis.

2.1 The Study Region

Thailand is located in Southeast Asia on a latitude of 5º N to 21º N and a longitude of 97º E to 106º E. Climatologically, the country is classified as a tropical monsoon and tropical savanna with 18-34º C average temperature and over 1,500 mm. average rainfall. The drought season ranges from November to January (winter) and February to April (summer). The study region covers the whole country.

2.2 Satellite Datasets

Satellite images were received from the Chulabhorn Satellite Receiving Station (CSRS). The FY-2E data is received hourly through the Digital Video Broadcast via Satellite (DVB-S) system from National Satellite Meteorological Center (NSMC) in Beijing while the Terra/Aqua MODIS data is received from the MODIS direct broadcast receiving the station at CSRS. In total, there are 1000*1600 pixels for each image, covering Thailand's entire territory, at 1 km/pixel spatial resolution.

2.2.1 FY-2E Dekadal rain estimate

Satellite data received through the DVB-S system is in a VSR file format. Upon received, these data are automatically transformed, using Equal-Lat-Long projection, to numerical data (16-bit PNG). Only a data point within the country region is retrieved and stored as a zip file every hour. Hourly satellite rain estimate is calculated from IR1 data using the Infrared Threshold Rainfall with Probability Matching (ITRPM) model [23]. The model was adjusted to provide dekadal rainfall by calibrating the satellite rain estimates accumulated in 10 days with co-located rain gauges accumulated rainfall from Thaiwater.net using a dataset in 2016. Fig. 1 (left) shows an example of an IR1 image from the FY-2E satellite that is used to calculate the dekadal rain estimate shown in Fig. 1 (right).

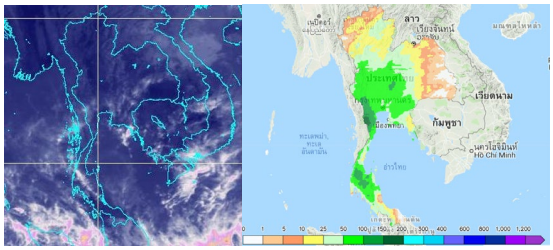

Fig. 1 Example of (left) an IR1 image from FY-2E satellite (right) corresponding FY-2E dekadal rain estimate

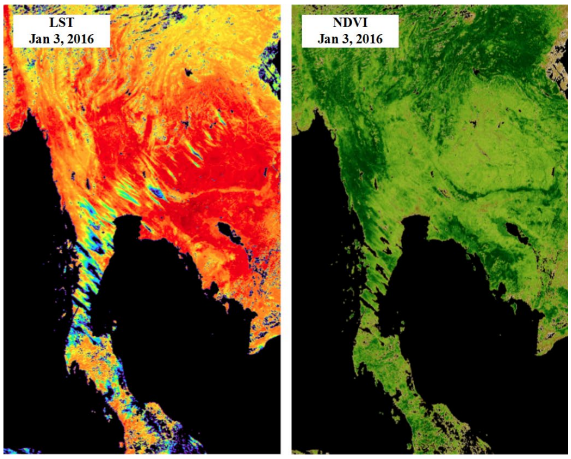

Fig. 2 Example of MODIS L2 products (left) LST (right) NDVI

2.2.2 MODIS difference Land Surface Temperature

Land Surface Temperature (LST), a MODIS L2 product with 1 km spatial resolution, is retrieved twice a day during the day- and night-time. The difference between the day and night LST values relates to the water content in the soil and can, therefore, indicate drought conditions. Fig. 2 (left) shows an example of the MODIS LST product. Both day and night LST data are filtered by the cloud mask product. Every 10 days, the maxima of day and night LST are selected. This method is adopted from the Maximum Value Composite (MVC) technique, which is widely employed to improve analysis and reduce errors from the environment and atmosphere [24,25]. The difference between those maxima is then computed, becoming a dekadal deltaT to be used as an input parameter of the drought hazard model.

2.2.3 MODIS Normalized Difference Vegetation Index

The Normalized Difference Vegetation Index (NDVI) is also a MODIS L2 product representing the wellness of vegetation as shown in Fig. 2 (right). The NDVI product is additionally processed by cloud masking and the MVC technique, as shown in Fig. 3, to compute the dekadal NDVI to be used as the last input parameter of the drought hazard model.

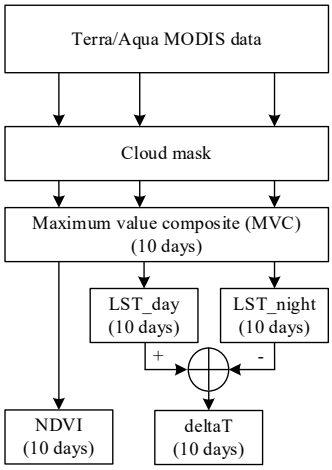

Fig. 3 Processing of Terra/Aqua MODIS data in providing dekadal NDVI and deltaT

2.3 Drought Hazard Model

In this work, drought hazard is defined as a composite drought assessment capturing three indicators that are not fully correlated with each other, including dekadal rain estimate from FY-2E satellite, dekadal deltaT and NDVI from MODIS sensors. These datasets were used as inputs of our drought hazard model. Daily soil moisture in-situ measurements collected in 2016 were obtained from the University of Phayao experimental site. Ten days-averaged soil moisture was used as a target for drought hazard model development by means of multiple linear regression approach, yielding $R^2 = 0.795$. Figure 4 shows the structure of the drought hazard model development. The drought hazard model is obtained as

$$DH = 11.643 + 0.356 * R - 0.297 * deltaT + 6.868 * NDVI \quad (1)$$

where R is the FY-2E dekadal rain estimate, $deltaT$ is the decadal difference LST and $NDVI$ is the dekadal NDVI, both from MODIS. A lower DH value implies worse drought conditions. This model works well during the dry season. However, in the rainy season, MODIS satellite data may not be available due to thick cloud cover. In this case, the drought hazard model is simplified as

$$DH = 12.445 + 0.135 * R \quad (2)$$

Since this model uses only dekadal estimated rainfall, the output of multiple linear regression yields lower $R^2 = 0.371$.

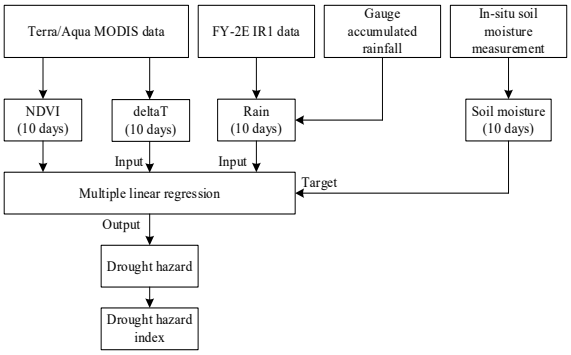

Fig. 4 Development of the drought hazard model

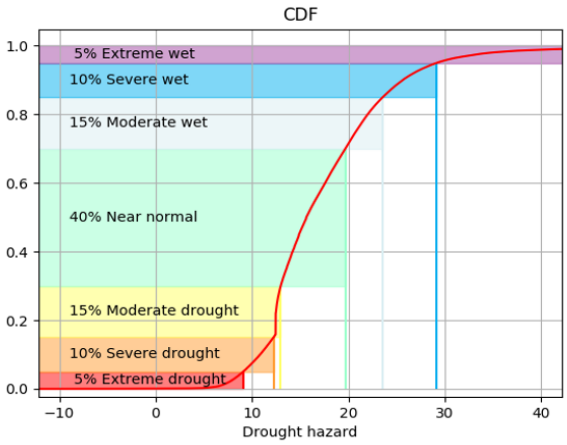

Fig. 5 Mapping between Drought Hazard CDF thresholds and DHI

2.4 Drought Hazard Index

The cumulative distribution function (CDF) of drought hazard is generated using sample values computed from satellite datasets observed in 2016. The CDF is grouped into seven threshold levels (presently at 0.05, 0.15, 0.30, 0.70, 0.80, and 0.95) to define the drought hazard index (DHI), which is represented by integer values ranging from –3 (extreme drought) to +3 (extreme wet). The thresholds corresponding to each DHI value are shown in Table 1. Drought hazard values are mapped to each DHI, representing the severity of drought conditions, based on the drought hazard CDF as shown in Fig. 5.

Table 1 Thresholds for the Drought Hazard Index

DH	Percentile	DHI
≤ 9.08	0 – 5	–3
9.08 – 12.23	5 – 15	–2
12.23 – 12.98	15 – 30	–1
12.98 – 19.69	30 – 70	0
19.67 – 23.57	70 – 85	1
23.57 – 29.14	85 – 95	2
> 29.14	95 – 100	3

2.5 Drought Risk Index

DHI is combined with a drought exposure index (EI) and drought vulnerability index (VI) to define drought risk for each province as

$$\boldsymbol{Drought\ Risk = DHI * EI * VI} \quad (3)$$

where $\boldsymbol{EI}$ is defined as the ratio of agricultural (crop and livestock) area to the total area of each province and $\boldsymbol{VI = 1 -}$ the fraction of irrigation area in each province. Examples of *EI* and *VI* for Bangkok, Chiang Mai, Ayutthaya, and Phuket provinces in 2016 are shown in Table 2 and 3, respectively.

Table 2 Examples of Drought Exposure Index

Province	Total Area (km^2)	Crop Area (km^2)	Livestock Area (km^2)	EI
Bangkok	1,566	267	111	0.24
Chiang Mai	22,041	5,240	34	0.24
Ayutthaya	2,547	1,870	45	0.75
Phuket	549	186	9	0.36

Table 3 Examples of Drought Vulnerability Index

Province	Total Area (km^2)	Irrigation Area (km^2)	VI
Bangkok	1,566	749	0.52
Chiang Mai	22,041	1,214	0.94
Ayutthaya	2,547	1,976	0.22
Phuket	549	1	0.99

Similar to DHI, drought risks are mapped, based on its CDF, to a seven-level drought risk index providing measures of the drought hazard impact in each area concerning its exposure to agricultural

damage and vulnerability in adaptation to drought disaster.

3. RESULTS AND DISCUSSIONS

To generate a drought hazard map every 10 days, the DHI for each pixel is calculated from the drought hazard model mapping with the CDF threshold. The drought hazard map is in a georeferenced raster format and can be displayed in a geographic information system (GIS) at 1 km spatial resolution. The results are qualitatively validated by the news about drought events and by agrometeorological reports from TMD (accumulated rainfall, MAI, and SMI). Quantitative validation of the model is performed based on the probability of detection (POD) for drought events that are officially announced by the Department of Disaster Prevention and Mitigation (DDPM), Ministry of Interior.

3.1 Comparison of Drought Hazard Map with Agrometeorological Reports

Result validation was qualitatively performed by comparison of the drought hazard map with the TMD agrometeorological reports in accordance with drought event news. All TMD reports are calculated from gauge station measurements and displayed in a portable document format (pdf) on the TMD website. A severe drought event was posted in the news at the beginning of January 2016 when there was a drought crisis, with extremely low water levels in the Bhumibol and Chaophraya dams located in the central region of Thailand. This event is clearly seen in the drought hazard map, Fig. 6 (a), showing severe to extreme drought in the central part of Thailand. This is confirmed by the accumulated rainfall, Fig. 6 (b), which exhibits light rainfall in the area.

Note that there are inconsistencies among TMD indices. For example, MAI map in Fig. 6 (c) indicates extreme drought almost throughout Thailand, whereas accumulated rainfall map shows a fair amount of rainfall in the southern part. However, the drought hazard map shows near normal to moderate drought conditions in that area, which is consistent with both accumulated rainfall and SMI maps, in Fig. 6 (a) and (d). Another example is the report for the eastern part that shows slightly less than normal rainfall, with moderate drought in the MAI map but severe drought in the SMI map. All this information was correctly accounted for in the drought hazard map with normal to moderate drought in the eastern area. Evidently, the drought hazard map is useful to monitor drought conditions coping with all three aspects including rainfall, vegetation and soil conditions. More importantly, it is much easier to interpret and to be comprehensible to the people in the area prone to drought risk, thus effectively supporting proactive drought management.

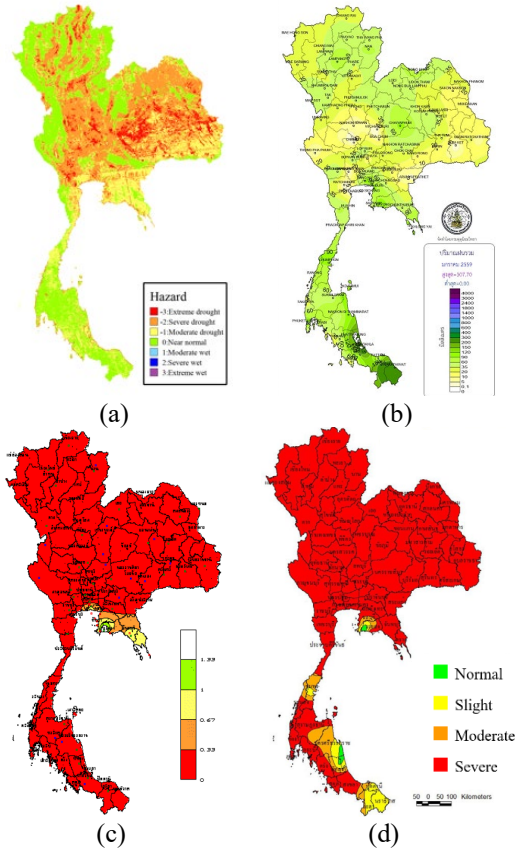

Fig. 6 Comparison of (a) drought hazard map, (b) accumulated rainfall, (c) moisture available index (MAI), and (d) soil moisture index (SMI) maps, during January 1–10, 2016

3.2 Probability of Detection (POD) Analysis

During the dry season (January to April) of 2016, the DDPM had announced 426 drought situations countrywide. Based on this information, the probability of detection (POD) of drought hazard for a drought event is calculated. Since the drought situation announcement is at the district level, the DHI values (with 1-km resolution) at the time of announcement were averaged over the relevant district area. For each announcement, a hit event occurs if the average DHI is less than –0.5. The probability of detection is computed by

$$POD = \frac{\text{total number of hit events}}{\text{total number of drought annoucement}} \quad (4)$$

The result was compared with the POD computed from the TMD report on MAI and SMI. The threshold for declaring drought by the MAI and

SMI is 2.5. Based on the level of MAI (0 – 4) and SMI (0 – 3), the average value over the district area was computed. If this value is less than 2.5, the hit event occurs. The results are shown in Table 4. The POD of DHI is 0.96, which is higher than the POD of MAI (0.91) but less than that of SMI (1.00).

Table 4 The probability of detection for drought hazard index (DHI), Moisture available index (MAI), and Soil moisture index (SMI).

Drought hit Thresholds	Number of hit events	POD
DHI < – 0.5	411	0.96
MAI < 2.5	388	0.91
SMI < 2.5	426	1.00

3.3 Comparison of Drought Hazard Map and Drought Risk Map

Derived from the drought hazard map, the drought risk map displays the corresponding regions affected by drought. However, the severity of drought is lessened where EI and/or VI are low and magnified where EI and/or VI are high. Shown in Figure 7 with a red circle, the drought risk index is slightly reduced compared with the drought hazard index in the northern forest region because of sparse agricultural areas. On the contrary, drought risk is magnified from drought hazard in the northeastern region where most areas are rain-fed agriculture with minor irrigation, shown as a blue circle in Fig. 7.

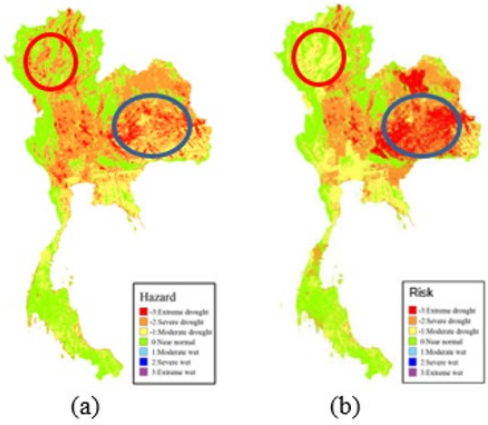

Fig. 7 Comparison of (a) drought hazard map and (b) drought risk map during January 1–10, 2016

3.4 Drought Risk Analysis Platform

To support practical drought monitoring and risk assessment and promote proactive drought management, a drought risk analysis platform is implemented. Shown in Figure 8, satellite inputs from TERRA/AQUA MODIS and FY-2 VISSR are received, processed and archived at the Chulabhorn Satellite Receiving Station (CSRS). Hourly Rainfall and daily LST products are kept in network storage to be processed as decadal products for the drought hazard and drought risk models. The output, stored in the Geoserver database, is ready to publish on the web server. Fig. 9 depicts user querying information from the platform via web service by selecting an area of interest, product types, and time.

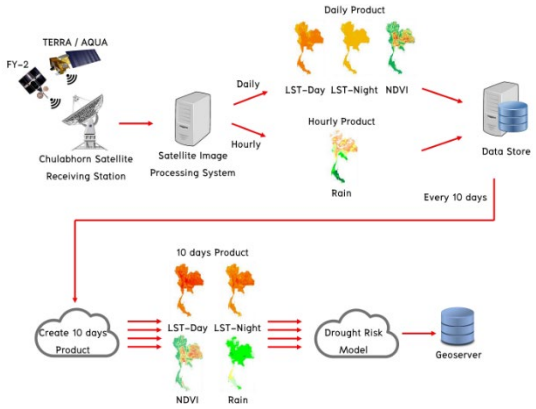

Fig. 8 Drought Risk Analysis Platform

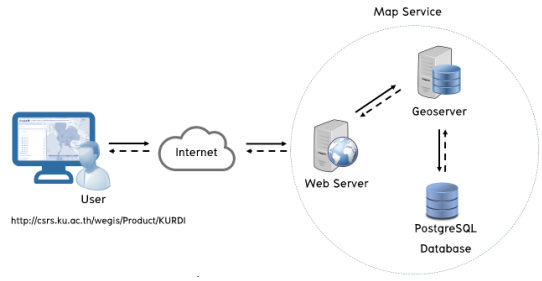

Fig. 9 User information query from the platform

4. CONCLUSIONS

This work presents a simple yet effective drought hazard model, integrating FY-2E and Terra/Aqua satellite data, for drought monitoring. Multiple linear regression is applied to develop the model with input parameters including accumulated rainfall estimate from FY-2E IR1 data and different LST and NDVI derived from Terra/Aqua MODIS data. These input parameters represent precipitation information, soil water content, and vegetation condition, respectively. Drought hazard can be calculated every 10 days at 1 km spatial resolution. The CDF of the drought hazard was then generated and used to assign the drought hazard index (DHI) with the thresholding method.

The results were qualitatively validated with drought crisis news. In comparison with the TMD agrometeorological reports, it is shown that a drought hazard index is a useful tool for drought monitoring in that it integrates all three drought aspects into one easy-to-understand index with consistent interpretation. Quantitatively, the results were validated against the DPM's drought situation announcement with a POD equals to 0.96.

The DHI is combined with drought exposure index (EI), represented by the agricultural areas, and drought vulnerability index (VI), calculated from the irrigation areas, to generate the drought risk values which are mapped to the drought risk index in a similar approach as DHI and posted as the drought risk map. As a result, drought risk assessment can be analyzed and represented by a seven-level drought risk index, which is illustrated by a drought risk map indicating the impact of drought hazard on agricultural areas based on its exposure and vulnerability. Both the drought hazard map and the drought risk map are automatically generated and published on the web at http://csrs.ku.ac.th/wegis/Product/KURDI (every 10 days). This information is beneficial to both the government and farmers, leading to proactive drought management.

5. ACKNOWLEDGMENTS

This research was supported by "Advancing Co-design of Integrated Strategies with Adaptation to Climate Change in Thailand (ADAP-T)" supported by the Science and Technology Research Partnership for Sustainable Development (SATREPS), JST-JICA and by the Kasetsart University Research and Development Institute (KURDI) under the project "A Development of Drought Risk Analysis Platform using Multiple Satellite Sensors".

6. REFERENCES

[1] AghaKouchak A., Farahmand A., Melton F., Teixeira J., Anderson M., Wardlow B., and Hain C., Remote sensing of drought: Progress, challenges and opportunities. NASA Publications, Nebraska-Lincoln, 2015.

[2] Zargar A., Sadig R., Naser B., and Khan F. I., A review of drought indices. Environmental Reviews, pp. 333-349, 2011.

[3] Sadegh M., Love C., Farahmand A., Mehran A., Tourian M.J., and AghaKouchak A., Multi-Sensor Remote Sensing of Drought from Space. Remote Sensing of Hydrological Extreme, Springer International Publishing Switzerland, 2017, pp. 219-236.

[4] Senay G. B., Velpuri N. M., Bohms S., Gudde M. Y. C., Rowland J., and Verdin J. P., Drought Monitoring and Assessment: Remote Sensing and Modeling Approaches for the Famine Early Warning Systems Network. Hydro-Meteorological Hazards, Risks, and Disasters, Nebraska-Lincoln, USGS Staff--Published Research, 2015, pp. 233-262.

[5] Carrao H., Naumann G., and Barbosa P. Mapping global patterns of drought risk: An empirical framework based on sub-national estimates of hazard, exposure and vulnerability. Global Environmental Change, vol. 39, pp. 108-124, 2016.

[6] Li X., Wang Y., Tang S., and Shen S., NDVI-LST Feature Space Based Drought Monitoring using MERSI Data in Hunan Province of China. International Conference on Geoinformatics (GEOINFORMATICS), Hong Kong, China, 2012.

[7] Sorooshian S., Hsu K., Gao X., Gupta H., Imam B., and Braithwaite D., Evaluation of the PERSIANN system satellite-based estimates of tropical rainfall. Bulletin of the American Meteorological Society, vol. 81, no. 9, p. 2035–2046, 2000.

[8] Huffman G. J., Bolvin D. T., Nelkin E. J., and Wolff D. B., The TRMM Multisatellite Precipitation Analysis (TMPA): Quasi-Global, Multiyear, Combined-Sensor Precipitation Estimates at Fine Scales. American Meteorological Society, vol. 8, pp. 38-55, 2007.

[9] Joyce R. J., Janowiak J.E., Arkin P.A., and Xie P., CMORPH: A Method that Produces Global Precipitation Estimates from Passive. JOURNAL OF HYDROMETEOROLOGY, vol. 5, pp. 487-503, 2004.

[10] Kubota T., Shige S., Hashizume H., Aonashi K., Takahashi N., Seto S., Hirose M., Takayabu Y. N., Nakagawa K., Iwanami K., Ushio T., Kachi M., and Okamoto K., Global Precipitation Map using Satelliteborne Microwave Radiometers by the GSMaP Project: Production and Validation. IEEE Transactions on Geoscience and Remote Sensing, vol. 45, no. 7, pp. 2259-2275, 2007.

[11] Kogan F., Application of vegetation index and brightness temperature for drought detection. Advances in Space Research, vol. 15, no. 11, pp. 91-100, 1995.

[12] Mc Vicar P.N. and Bierwirth R., Rapidly assessing the 1997 drought in Papua New Guinea using composite AVHRR imagery. *International Journal of Remote Sensing,* vol. 22, pp. 2109-2128, 2001.

[13] Tucker C., Red and photographic infrared linear combinations for monitoring vegetation. remote sensing of environment, vol. 8, no. 2, pp. 127-150, 1979.

[14] Park J.S., Kim, K.T. and Choi, Y.S., Application of vegetation condition index and

standardized vegetation index for assessment of spring drought in South Korea. Geoscience and Remote Sensing Symposium, Boston, Mass, 2008.

[15] Kogan F. and Sullivan J., Development of the global drought-watch system using NOAA/AVHRR data. Advances in Space Research, vol. 13, no. 5, pp. 219-222, 1993.

[16] Karnifli A., Agam N., Pinker T. R., Anderson M., Imhoff M.L., Gutman G.G., Panov N. and Goldberg A., Use of NDVI and land surface temperature for drought assessment: Merits and Limitations. Journal of Climate, vol. 23, pp. 618-633, 2010.

[17] Senay G B., Velpuri N M., Bohms S., Gudde M., Young C., Rowland J., and Verdin J. P., A Simple Interpretation of the Surface Temperature/vegetation Index Space for Assessment of Surface Moisture Status. Remote Sensing of Environment, vol. 79, no. 2-3, pp. 213-224, 2002.

[18] Wang P.X., Wan Z.M., and Gong J.Y., Advances In Drought Monitoring by Using Remotely Sensed Normalized Difference Vegetation Index and Land Surface Temperature Products. Advance In Earth Sciences, vol. 18, no. 4, pp. 527-533, 2003.

[19] Fan G. Zhang Y., He Y., and Wang K., Risk Assessment of Drought in the Yangtze River Delta Based on Natural Disaster Risk Theory, Hindawi, Discrete Dynamics in Nature and Society, Vol. 2017.

[20] Kim H., Park J., Yoo J., Kim T.W., Assessment of drought hazard, vulnerability, and risk: A case study for administrative districts in South Korea, Journal of Hydro-environment Research, Vol.9, Issue 1, 2015, pp. 28-35.

[21] Jiang S., Yang R., Cui N., Zhao L., and Liang C., Analysis of Drought Vulnerability Characteristics and Risk Assessment Based on Information Distribution and Diffusion in Southwest China. The atmosphere, vol. 9, 2018.

[22] Carrao H. and Barbosa P., Models of Drought Hazard, Exposure, Vulnerability and Risk for Latin America. European Commission – Joint Research Center, 2015.

[23] Veerakachen W. and Raksapatcharawong M., Rainfall estimation for real-time flood monitoring using geostationary meteorological satellite data," Advances in Space Research, vol. 56, no. 6, pp. 1139-1145, 2015.

[24] Holben B., Characteristics of maximum-value composite images from temporal AVHRR data. International Journal of Remote Sensing, vol. 7, pp. 1417-1434, 1986.

[25] Liu H., Zhang A., Jiang T., Lu H., Liu X., and Wang H., The Spatiotemporal Variation of Drought in the Beijing-Tianjin-Hebei Metropolitan Region (TTHMR) Based on the Modified TVDI. Sustainability, vol. 8, pp. 1-15, 2016.